ChemPubSoc Europe

DOI: 10.1002/cssc.201600572

CHEMSUSCHEM Full Papers

VIP *Very Important Paper*

Ag-Promoted ZrBEA Zeolites Obtained by Post-Synthetic Modification for Conversion of Ethanol to Butadiene

Vitaly L. Sushkevich[a] and Irina I. Ivanova*[a, b]

1,3-Butadiene was synthesized from ethanol using zirconium-containing zeolite beta (ZrBEA) catalysts doped with 1 wt% silver. The Zr was planted using post-synthesis modification by dealumination of the parent zeolite followed by treatment with $ZrOCl_2$ in a DMSO solution. FTIR and NMR spectroscopy were used to investigate the planting process by preparing materials with different Si/Al ratios and crystal sizes. The results showed preferential grafting of Zr to the terminal silanols present on the external surface of the zeolite crystals instead of incorporation of Zr into silanol nests. The grafting yielded highly accessible $Zr(OSi)_3OH$ open sites with high Lewis acidity, as confirmed by FTIR spectroscopy of adsorbed CO. These sites are shown to be extremely active for the conversion of ethanol to butadiene. Ag/ZrBEA catalysts prepared using the post-synthesis method showed significant advantages compared with Ag/ZrBEA catalysts synthesized using a conventional hydrothermal procedure. The best catalyst performance in terms of butadiene formation rate (3 $\mu mol\,g^{-1}\,s^{-1}$) was observed over Ag/Zr(3.5)BEA(75) (containing 3.5 wt% Zr), which had the smallest crystal size and the highest content of Zr open sites of the prepared catalysts.

Introduction

The recent discovery of metallosilicates such as Sn-, Zr-, and Ti-substituted zeolites has opened new possibilities for the development of environmentally friendly solid Lewis acid catalysts for sustainable chemistry.[1–7] These materials have been applied as catalysts in various reactions for the conversion of biomass-derived compounds, including Baeyer–Villiger oxidation and Meerwein–Ponndorf–Verley–Oppenauer (MPVO) reduction reactions,[8–11] aldol condensation,[12,13] carbohydrate isomerization and epimerization,[14–20] Cannizzaro-type reactions,[21–23] and butadiene synthesis from ethanol.[24,25] The latter process has attracted a lot of attention in the past decade owing to its industrial applications.

Nowadays, butadiene is an important industrial monomer used for the production of rubbers, plastics and different chemicals. Typically, it is obtained as a co-product from naphtha crackers used for ethylene and propylene production. However, the increased production of shale gas has led to a lightening of the feedstocks for steam crackers and has resulted in a shortage of longer-chain hydrocarbons in pyrolysis products, including butadiene. Therefore the development of an alternative, cheap, and sustainable process for the synthesis of butadiene from biomass feedstocks is highly desirable.[26–29] A wide variety of catalytic systems have been synthesized and tested for the conversion of ethanol into butadiene, including bulk and mixed oxides, clay materials, and zeolites.[28,29] Recent studies performed by our group have indicated that the silver-promoted Zr-containg zeolite beta (ZrBEA) is among the most efficient catalysts for the conversion of ethanol to butadiene.[24,25]

However, to achieve widespread industrial application of ZrBEA, a thorough improvement of its synthesis is needed. Current synthesis procedures use corrosive and toxic hydrogen fluoride (HF) in the synthesis gel and the hydrothermal synthesis takes up to 30 days to ensure crystallization of zeolite BEA with high Zr content in the framework.[11,24,30] Moreover, the large ZrBEA crystals formed under these conditions may face mass transfer limitations during the catalytic processes.

Post-synthesis is a useful alternative route for implanting transition metal ions into a zeolite framework. There have been many examples of the preparation of metallosilicates through the reaction of highly siliceous zeolites with metal chloride vapors. This so-called "atom-planting method" has proven to be an efficient way of incorporating Al, Ga, Sb, As, In and Ti into the zeolite framework types MFI, MOR, and BEA.[31–35] It has also been applied successfully for the post-synthesis of SnBEA catalysts by solid–gas reaction of dealuminated BEA with tin chloride,[36,37] tin acetate,[22] and various organometallic compounds.[38] Another approach, which uses the deposition of $SnCl_4$ in dried isopropanol under reflux conditions, has been proposed by Sels et al.[19,39–41] This method avoids the application of vapor phase deposition and the formation of a large amount of extra framework tin oxide.

[a] Dr. V. L. Sushkevich, Prof. I. I. Ivanova
Department of Chemistry
Lomonosov Moscow State University
Leninskye Gory 1, bld. 3, 119991 Moscow (Russia)
Fax: (+7) 495-939-3570
E-mail: iiivanova@phys.chem.msu.ru

[b] Prof. I. I. Ivanova
A.V. Topchiev Institute of Petrochemical Synthesis
Russian Academy of Science
Leninskiy prospect, 29, 119991 Moscow (Russia)

Supporting Information for this article can be found under http://dx.doi.org/10.1002/cssc.201600572.

In contrast to SnBEA, post-synthesis of ZrBEA is not well documented in the literature. Recently, Tang et al. reported a post-synthetic strategy leading to mesoporous ZrBEA by dealumination, desilication and incorporation of Zr. However, expensive zirconium cyclopentadienyl compounds were used for Zr deposition.[42] Wolf et al. used zirconium ethoxide (less expensive but sensitive to water) for a solid state exchange reaction to incorporate Zr atoms into the framework.[43] Therefore, the development of a simple procedure for post-synthesis of ZrBEA using cheaper and stable precursors is an important goal.

Here, we report a simple and cheap synthetic route for the synthesis of ZrBEA by the treatment of dealuminated BEA zeolites with $ZrOCl_2$ in dimethyl sulfoxide (DMSO) under reflux conditions. This procedure yields ZrBEA catalysts with high content of open Zr Lewis sites, as confirmed by FTIR spectroscopy of adsorbed CO. When doped with Ag, the catalysts showed extremely high catalytic performance for the synthesis of butadiene from ethanol. Comparison with Ag/ZrBEA catalysts synthesized by the conventional hydrothermal procedure indicates that the proposed post-synthetic method has significant advantages.

Results and Discussion

Structure, texture and morphology of the catalyst

The chemical and textural characteristics of the parent and modified zeolites are presented in Table 1. The parent zeolites include a series of highly crystalline BEA samples with Si/Al = 19, 25, 38, and 75 [BEA(*x*), where *x* is the Si/Al ratio]. Nitrogen adsorption–desorption data showed an equal micropore volume (0.16 $cm^3 g^{-1}$) for all the parent samples, whereas the total pore volume differed substantially between 0.31–0.75 $cm^3 g^{-1}$ (Table 1). The nitrogen adsorption–desorption isotherms (Figure S1, Supporting Information) showed an increase of N_2 uptake at high relative pressures owing to the increase of the intercrystalline porosity in the samples in the order BEA(19) < BEA(25) < BEA(38) < BEA(75). This observation indicated that the crystal size of the catalysts decreases in the same order. These results were confirmed by SEM analysis of the parent zeolites (Figure 1). Indeed, the average crystal size increased from 50 nm for BEA(75) up to 300 nm for BEA(19).

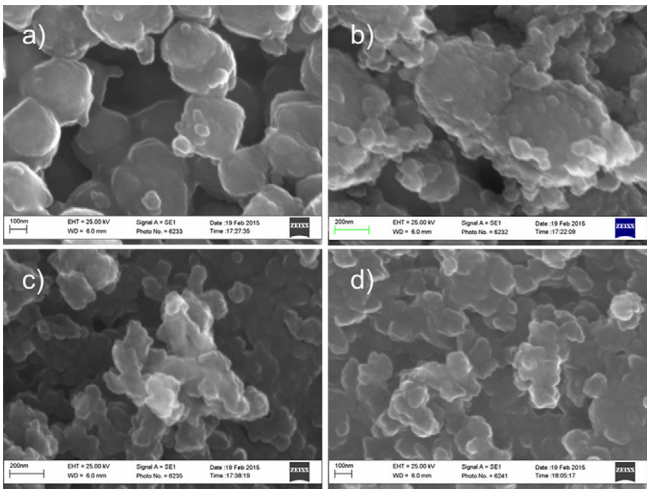

Figure 1. SEM images of a) BEA(19), b) BEA(25), c) BEA(38) and d) BEA(75) (scale bars correspond to 100 (a, c) and 200 nm (b, d)).

Dealumination of AlBEA zeolites was performed using a procedure that does not lead to any significant destruction of the zeolite.[44] The standard procedure proposed in Ref. [44] takes 20 h and uses 13 M HNO_3 at 373 K for the complete removal of aluminum. In the present work, we used slightly milder conditions including slightly diluted nitric acid and a lower temperature. The dealumination procedure was repeated four times and the resultant samples were essentially free of Al. The dealumination of the zeolites did not lead to any significant changes in their structure and texture. A slight decrease in the micropore volume and an increase in the mesopore volume was observed (Table 1) owing to the removal of Al atoms from the zeolite framework but the pore structure remained largely intact. SEM images (Figure S3 b) showed that the dealumination resulted in slight destruction of the zeolite crystal agglomerates.

The incorporation of zirconium into the framework of dealuminated zeolites was performed in DMSO using $ZrOCl_2$ as a precursor. DMSO was chosen as a solvent owing to the high solubility of zirconyl chloride. Furthermore, DMSO prevents the polymerization of ZrO^{2+} cations in solution and relieves the interaction of Zr with the silanol groups of the zeolite. The SEM images (Figure S3 c) indicate that Zr grafting does not lead to any changes in the catalyst morphology. It should be noted that ZrBEA samples obtained by post-synthetic treatment show a larger mesopore volume than the hydrothermally synthesized benchmark sample ZrBEA-HT (Table 1) owing to the smaller zeolytic crystals of the former. As confirmed by SEM, the hydrothermally synthesized ZrBEA-HT sample had large crystals with a size above 5 μm and a broad size distribution (Figure S2).

The structure of the catalysts before and after treatments was analyzed by XRD (Figure 2). The

Table 1. Catalyst characteristics.

Sample	Si/Al ratio	Si/Zr ratio	BET [$m^2 g^{-1}$]	Total pore volume [$cm^3 g^{-1}$]	Micropore volume [$cm^3 g^{-1}$]
BEA(19)	19	–	495	0.31	0.16
BEA(25)	25	–	530	0.45	0.16
BEA(38)	38	–	510	0.66	0.16
BEA(75)	75	–	525	0.75	0.16
DeAlBEA(19)	traces	–	505	0.33	0.15
DeAlBEA(25)	traces	–	520	0.48	0.15
DeAlBEA(38)	traces	–	520	0.68	0.15
DeAlBEA(75)	traces	–	515	0.76	0.15
Zr(1.3)BEA(19)	traces	157	505	0.33	0.15
Zr(2.1)BEA(25)	traces	97	520	0.48	0.15
Zr(3.3)BEA(38)	traces	63	515	0.68	0.15
Zr(3.5)BEA(75)	traces	59	520	0.76	0.15
Zr(1.5)BEA-HT	n/a	130	470	0.31	0.20

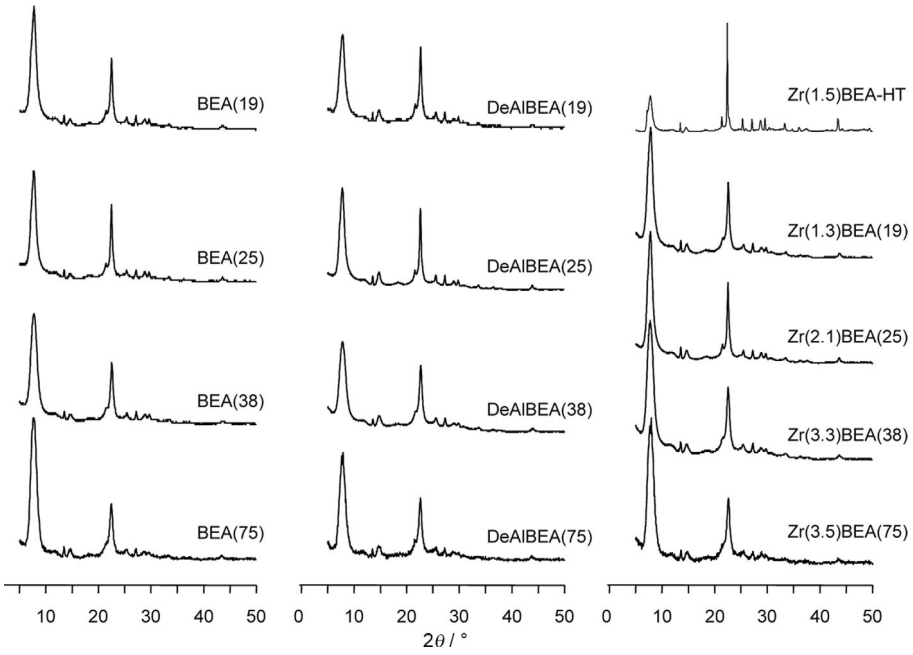

Figure 2. XRD patterns of the catalysts.

powder XRD patterns of BEA, DeAlBEA and ZrBEA samples show typical features of crystalline zeolite BEA. No peaks of crystalline ZrO_2 or any other crystalline impurity phases were detected. All ZrBEA samples synthesized by dealumination of AlBEA zeolites exhibited broader XRD patterns with respect to the conventional ZrBEA-HT, which is in line with SEM measurements and indicated the significantly larger crystals in the case of hydrothermally synthesized ZrBEA.

Chemical state and location of Zr atoms

It is generally accepted that the mechanism of post-synthetic planting of heteroatoms in the framework of zeolites involves the formation of so-called silanol nests through the dealumination of AlBEA followed by the interaction of these silanol nests with the metal source leading to tetrahedral metal sites incorporated into the zeolite framework (Scheme 1).[34–43] Based on these literature hypotheses, we were expecting that an increase of the Al content in the parent BEA zeolite would lead to a higher amount of silanol nests and therefore a higher degree of Zr incorporation. However, the opposite tendency was observed (Table 1). The decrease of the Si/Al ratio from 75 to 19 in the parent zeolite led to an increase of the Si/Zr ratio from 59 to 157 in ZrBEA materials. This unexpected behavior prompted us to investigate other possible mechanisms for Zr planting using NMR and IR spectroscopy.

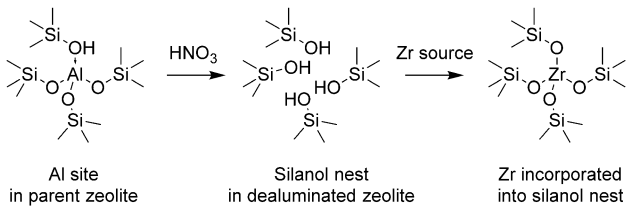

Scheme 1. Generally accepted scheme for post-synthesis modification of zeolites by dealumination followed by incorporation of heteroatoms.

^{29}Si magic angle spinning (MAS) NMR spectra presented in Figure 3 show the evolution of the silicon environment during dealumination and Zr planting. The ^{29}Si MAS NMR spectra of the parent zeolites show NMR peaks in the regions from −113 to −110 ppm and from −104 to −102 ppm. The former signals correspond to Si atoms in $Si(OSi)_4$ species in nonequivalent T crystallographic sites of BEA (9 sites), which are not well resolved. The latter signals are owing to overlapping lines of $(SiO)_3Si(OAl)$ and $(SiO)_3Si(OH)$ species. The presence of the latter is confirmed by the appearance of the signal at approximately 101.5 ppm in the ^{1}H–^{29}Si cross-polarization (CP)MAS NMR spectra (Figure S4).

The $Si(OSi)_4$ signals in the region of −110 to −113 ppm do not change after dealumination, confirming that the zeolite structure remains intact. However, the $(SiO)_3Si(OAl)$ signal at approximately −103.5 ppm disappears, which is a clear indication of the aluminum leaching from the parent material. At the same time, the signal at −101.5 ppm increases owing to the formation of $(SiO)_3Si(OH)$ defects.[39–41] This observation is confirmed by ^{1}H–^{29}Si CPMAS NMR spectra (Figures S4 and S5), which point to the formation of new Si–OH groups.

After grafting of Zr, the relative intensity of the signal at approximately −101.5 ppm decreases in both the one-pulse (Figure 3) and CPMAS NMR (Figure S4) spectra, indicating partial consumption of the silanol groups during the post-synthesis treatment. Therefore, NMR data indicated that there was an interaction between the Zr atoms and the silanol groups, but this method did not allow us to determine the type of silanol

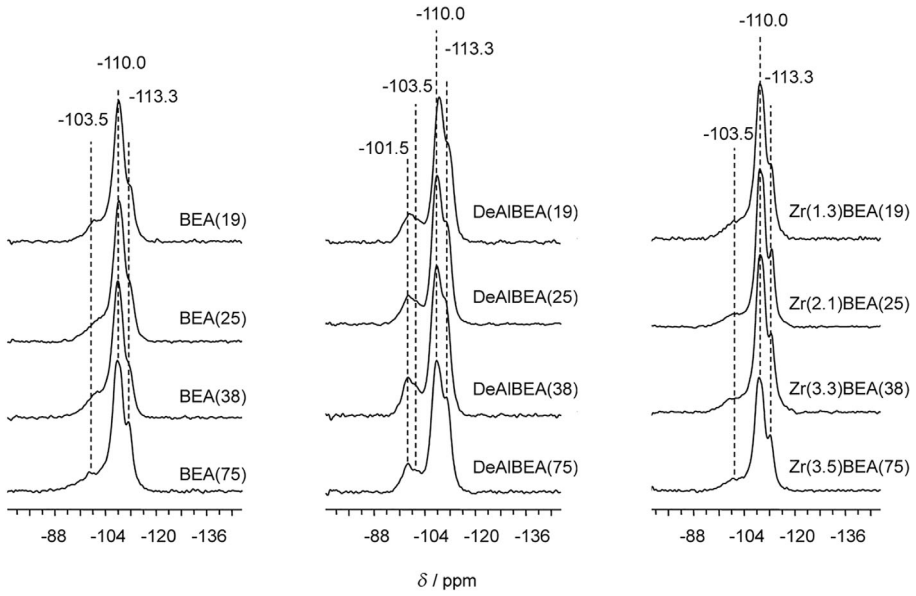

Figure 3. ^{29}Si MAS NMR spectra of the catalysts.

involved in the grafting. This information can be best obtained by FTIR spectroscopy.

Figure 4 shows the FTIR spectra in the region of the hydroxyl groups vibrations of the parent zeolites, dealuminated samples and ZrBEA catalysts. The bands at approximately 3608 cm^{-1} and 3783 cm^{-1} were assigned to Brønsted acid sites and non-framework Al–OH, respectively. A broad signal at approximately 3660 cm^{-1} was attributed to the perturbed Al–OH. The sharp intense band at 3745 cm^{-1} was attributed to O–H vibrations in terminal isolated silanol groups.[45,46] It should be noted that the relative intensity of this band for the samples increased in the order BEA(19) < BEA(25) < BEA(38) ≈ BEA(75), indicating an increase of the content of terminal silanols. This observation could be associated with the decrease of the size of zeolite crystals, as confirmed by SEM (Figure 1) and nitrogen adsorption measurements (Figure S1).

After dealumination, the signals at 3783, 3660 and 3608 cm^{-1} disappeared and a broad band spanning from 3750 to 3400 cm^{-1} appeared (Figure 4). This band originates from hydrogen bonded silanols, that is, silanol nests.[34–43] A slight increase of the intensity of the band at 3745 cm^{-1} indicated that there was partial destruction of the zeolite crystal aggregates

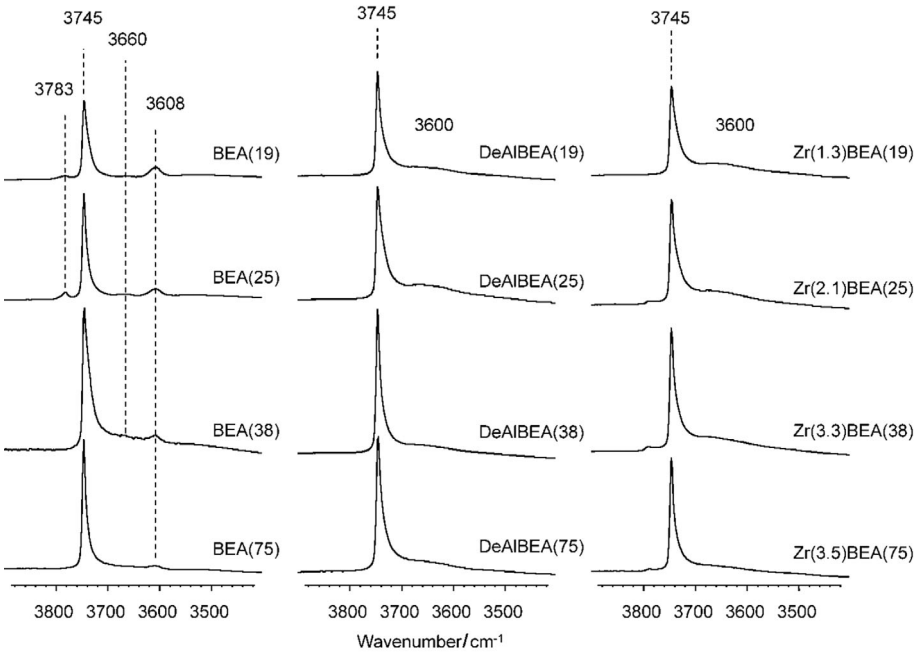

Figure 4. FTIR spectra showing the OH vibration region.

followed by the formation of isolated Si–OH groups on the surface (Figure S5).

The introduction of Zr resulted in a decrease of the 3745 and 3600 cm^{-1} bands (Figures 4 and S5) owing to the interaction of the corresponding silanols with $ZrOCl_2$ and the formation of Zr sites. A careful analysis of the intensities of these bands (Figure S5) showed that the treatment of dealuminated zeolite in the $ZrOCl_2$ solution leads to the preferential consumption of isolated terminal silanol groups and only a slight decrease in the amount of silanol nests. These results indicate the preference of the Zr atoms to graft on the surface of the zeolite rather than incorporate into the silanol nests.

To further clarify the mechanism of Zr planting, the intermediate products obtained at different stages of the post-synthesis procedure were analyzed (Figure 5). Two alternatives

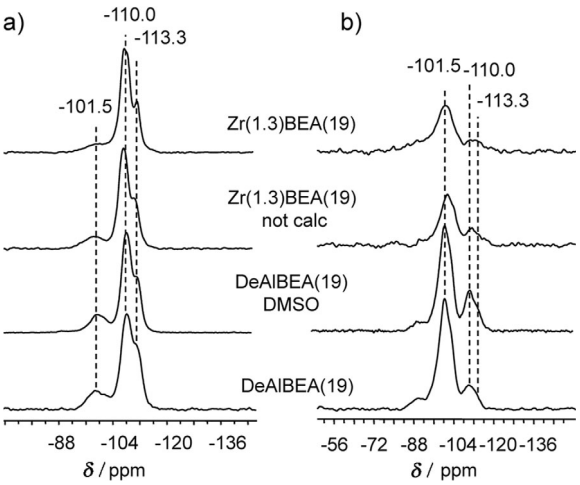

Figure 5. a) ^{29}Si MAS NMR and b) ^{1}H–^{29}Si CPMAS NMR spectra of DeAlBEA and Zr(1.3)BEA(19) catalysts.

were considered: i) grafting of Zr during the treatment of DeAlBEA with $ZrOCl_2$ in DMSO solution and ii) adsorption of Zr species on DeAlBEA [the different samples are DeAlBEA(*x*) where *x* is Si/Al ratio in the parent zeolite] during the treatment in DMSO solution followed by grafting to silanol groups during the calcination process.

^{29}Si MAS NMR (Figure 5a) and ^{1}H–^{29}Si CPMAS NMR (Figure 5b) spectra of DeAlBEA(19), DeAlBEA(19) treated in pure DMSO, DeAlBEA(19) treated with $ZrOCl_2$ in DMSO and calcined Zr(1.3)BEA(19) (the number after Zr corresponds to the Zr content) samples were obtained. The comparison of the spectra indicates that treatment in pure DMSO does not have a significant effect on the peak at approximately −101.5 ppm corresponding to the Q^3 resonance of $(SiO)_3Si(OH)$ groups. On the contrary, the intensity of this peak decreased drastically after the addition of $ZrOCl_2$ to DMSO, whereas further calcination does not affect the spectrum. These observations indicate that the interaction of the silanol groups with the Zr source occurs during the treatment of the zeolite with $ZrOCl_2$ in the DMSO solution and that the subsequent calcination does not affect the Zr sites.

In summary, the NMR and FTIR data suggest that the introduction of Zr into the DeAlBEA samples is associated with preferable consumption of the terminal isolated silanols during the treatment in $ZrOCl_2$ solution, whereas the silanol nests are not affected significantly. The amount of planted Zr atoms correlates with the amount of isolated Si–OH groups located on the external surface of the crystal. The latter observation suggests that treatment of dealuminated zeolite BEA with $ZrOCl_2$ in DMSO leads to grafting of the Zr atoms predominantly on the external surface of the crystal or in the mouths of the pore close to the external surface (Scheme 2), which is favored on smaller zeolite crystals.

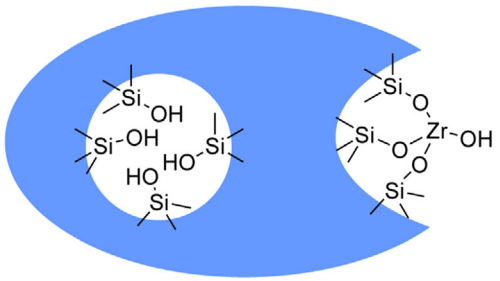

Scheme 2. Schematic representation of Zr grafting by treatment of dealuminated zeolites with $ZrOCl_2$ in DMSO.

Several reasons can be proposed to account for such behavior of zirconium during grafting: i) diffusion limitations of the solvated ZrO^{2+} species in the porous system of the zeolite; ii) steric hindrance, which restricts the formation of four Si–O–Zr linkages in silanol nests owing to the larger atomic size of Zr with respect to Al, and iii) energetically unfavorable formation of $Zr(OSi)_4$ species in the silanol nests formed after dealumination.

Acidic properties

The catalytic properties of ZrBEA materials are closely related to their Lewis acidity. FTIR spectroscopy of adsorbed pyridine is usually used for the characterization of Lewis acid sites.[30,42] However, pyridine is a not very sensitive probe molecule for different types of Lewis acid sites and OH groups and does not allow for the determination of their nature and strength. In our previous study[47] we showed that the use of CO for the examination of the acidic properties of ZrBEA catalysts is more beneficial owing to the high sensitivity of carbon monoxide as a probe molecule.

Therefore, the nature of the ZrBEA acid sites was investigated by FTIR spectroscopy of CO adsorbed at low temperature.[47,48] The adsorption of CO on the acidic catalysts leads to the formation of hydrogen bonds with the OH groups and to coordination of CO to the Lewis acid sites. Because of these interactions the ν(C=O) vibration band of adsorbed carbon monoxide shifts to higher wavenumbers with respect to the band of physisorbed CO (2138 cm^{-1}). This shift is characteristic of the nature (Lewis or OH) and strength of the site. Furthermore,

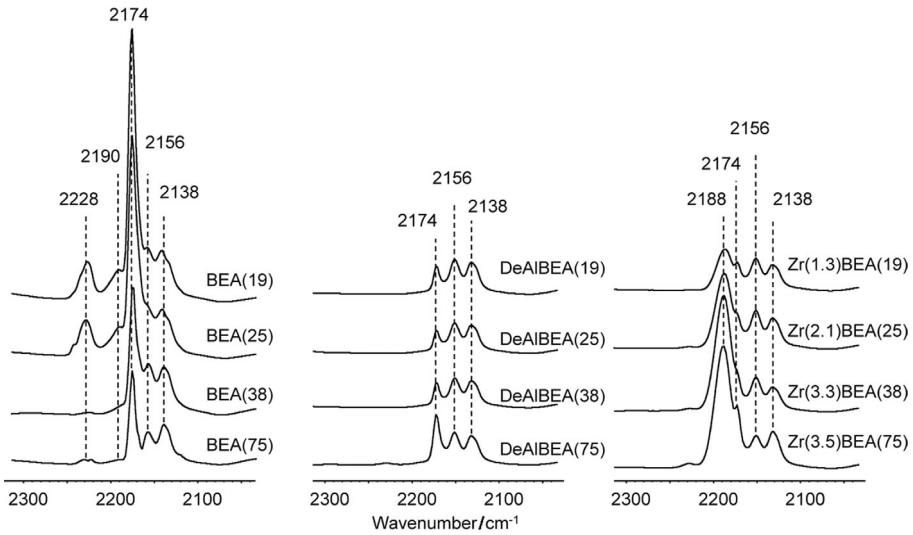

Figure 6. FTIR spectra of CO adsorbed over the catalysts.

CO can easily access all the sites because of its small size. This has an additional advantage for the investigation of the acidity of microporous solids.[48]

In a typical experiment, carbon monoxide was gradually introduced in the IR cell and the adsorption spectra were collected. The experiment was stopped after the appearance of the band of physisorbed CO (2138 cm^{-1}) in the spectra. The results obtained after saturation are shown in Figure 6. The adsorption of CO over BEA samples led to the appearance of bands at 2228, 2190, 2174 and 2156 cm^{-1} (Figure 6). The bands at 2228 and 2190 cm^{-1} was attributed to the vibrations of CO adsorbed over Al Lewis sites in tetrahedral (Al_{4c}^{3+}) and octahedral (Al_{6c}^{3+}) positions, respectively.[49] An intense band at 2174 cm^{-1} is typical of the adsorption of CO over Brønsted acid sites Si–O(H)–Al,[45,48] and finally, the band at 2156 cm^{-1} was assigned to the vibrations of CO interacting with silanol groups on the surface of the zeolites.[48] BEA samples with a low Si/Al ratio showed a high amount of Al Lewis acid sites (Figure 6), indicating a high concentration of crystal defects owing to the high aluminum content.

The amount of CO adsorbed was quantified using a curve-fitting procedure for the FTIR spectra that is based on the application of Gauss–Lorentz components with a fixed full width at half maximum centered at the maxima of the bands. The results are shown in Table 2. The intensity of the band at 2174 cm^{-1} correlates with the number of Al atoms in the BEA samples and shows that there was an increase in the amount of Brønsted sites with the increase of aluminum content. The BEA(38) and BEA(75) samples do not show any Lewis acid sites, which indicates that all the aluminum atoms were incorporated into the framework and confirms the high quality of the parent materials.

Dealumination of the BEA samples caused a dramatic decrease in the amount of acid sites. The amount of Brønsted acid sites decreased by two orders of magnitude as compared to the parent BEA zeolites, whereas the Lewis sites disappear completely. However, it has to be noted that leaching with nitric acid four times did not lead to complete dealumination of the zeolites. All DeAlBEA samples preserved some amount of Brønsted acid sites (Table 2).

The adsorption of CO over ZrBEA catalysts led to the appearance of a new band centered at 2188 cm^{-1}, which was attributed to CO interacting with Zr Lewis sites. According to our previous study,[47] this band corresponds to the open Lewis sites associated with Zr atoms linked to three oxygen atoms in the zeolite framework and one OH group. The intensity of the band corresponding to CO adsorbed on Zr open Lewis sites in the catalysts increases in the following order: Zr(1.3)BEA(19) < Zr(2.1)BEA(25) < Zr(3.3)BEA(38) ≈ Zr(3.5)BEA(75) (Table 2). This order of acidity correlates with the amount of Zr grafted on the external surface of the zeolite crystals (Table 1). The ZrBEA-HT sample showed the lowest amount of open sites (Table 2) and a considerable contribution from closed sites, as evi-

Table 2. Relative intensities of the IR bands observed after CO adsorption.

Sample	Area of band centered at		
	2228 cm^{-1} (Al^{3+} Lewis acid sites)	2174 cm^{-1} (Brønsted acid sites)	2188 cm^{-1} (Zr^{4+} Lewis sites)
BEA(19)	0.49	3.15	–
BEA(25)	0.46	2.77	–
BEA(38)	0.02	1.65	–
BEA(75)	0.02	1.12	–
DeAlBEA(19)	< 0.002	0.07	–
DeAlBEA(25)	< 0.002	0.06	–
DeAlBEA(38)	< 0.002	0.07	–
DeAlBEA(75)	< 0.002	0.10	–
Zr(1.3)BEA(19)	< 0.002	0.06	0.99
Zr(2.1)BEA(25)	< 0.002	0.07	1.50
Zr(3.3)BEA(38)	< 0.002	0.07	2.36
Zr(3.5)BEA(75)	< 0.002	0.11	2.49
Zr(1.5)BEA-HT	0.00	0.00	0.36

denced by the appearance of an intense band at 2176 cm^{-1} (Figure S6).[25,47]

Notably, the post-synthetic treatment with $ZrOCl_2$ in DMSO did not lead to the formation of closed Lewis sites, which are expected if Zr is incorporated into silanol nests (Scheme 1). The formation of only open sites confirmed our proposed mechanism of Zr deposition through grafting onto the isolated silanol groups (Scheme 2) rather than the incorporation into silanol nests.

Although a lot of effort has recently focused on the investigation of the nature of the acid sites in post-synthetically treated BEA materials,[19,23,34,36,38–42] the structure of the acid sites in these materials is still under debate. It is generally accepted that post-synthesis modification of dealuminated BEA zeolites can give both open and closed Lewis acid sites,[40–42] the structures of which have been proposed previously for hydrothermally synthesized SnBEA. However, in a recent paper by Dijkmans et al.[39] it was clearly demonstrated that the nature of the Sn sites introduced by a post-synthetic procedure can differ substantially from those obtained by hydrothermal synthesis. In particular, extended X-ray absorption fine structure (EXAFS) and X-ray absorption near edge structure (XANES) data pointed to 3-fold anchoring of Sn^{IV} and charge balancing by distant Si–O linkages. Our observations, which indicate the formation of highly accessible open Zr sites located near the external surface of the crystal (Scheme 2) are in line with these findings.

It has been repeatedly demonstrated that the open Lewis sites are the main active sites of the reactions studied over metal-substituted BEA catalysts (e.g., SnBEA, ZrBEA and TiBEA).[25,34,36,38,42] In our previous study we showed that Zr open sites are more active than closed sites in the synthesis of butadiene from ethanol.[25] Therefore, the formation of only $Zr(OH)(OSi)_3$ sites during the post-synthetic preparation of ZrBEA from dealuminated materials opens new possibilities for the design of catalysts with high intrinsic activity. In the present study, the activity of such catalysts was evaluated for the synthesis of butadiene from ethanol.

Evaluation of catalyst performance for the conversion of ethanol to butadiene

The main reaction products observed using the catalysts in this study were typically the same as in the previous study over metal-promoted oxide catalysts (Scheme 3).[49]

The main reaction pathway that leads to butadiene involves five reaction steps: i) ethanol dehydrogenation into acetaldehyde, ii) aldol condensation of acetaldehyde followed by iii) fast dehydration, iv) MPVO reduction of crotonaldehyde with ethanol and v) dehydration of crotyl alcohol into butadiene. Besides dehydrogenation, ethanol undergoes dehydration to give diethyl ether and ethylene. Furthermore, acetaldehyde is very reactive and initiates two side reactions: i) Tischenko reaction leading to ethyl acetate, which is further converted into acetone and propylene, and ii) cross-condensation with crotonaldehyde and other aldehydes leading to heavier products such as hexatrienes. Another side reaction pathway involves hydrogenation of crotyl alcohol to give 1-butanol and its further dehydration and isomerization into a mixture of butenes.

The catalytic properties of the parent, dealuminated and Zr-containing catalysts are compared in Figure 7 for BEA(75) zeolites. The parent and dealuminated zeolites show high initial rates of ethanol conversion, however the only reaction products obtained are ethylene and diethyl ether. When DeAl-BEA(75) is doped with Ag, significant dehydrogenation of ethanol into acetaldehyde is observed along with ethanol dehydration. However further transformation into butadiene does not occur because no Zr Lewis sites are present in the Ag/DeAl-BEA(75) catalyst. Grafting of Zr onto the dealuminated zeolite changes the reaction pathway towards butadiene synthesis owing to the successful incorporation of catalytically active Zr sites in the dealuminated zeolite.

To compare the activity of different Zr-containing catalysts, the initial rates of butadiene formation were estimated, as described in the Experimental Section; the results are presented in Table 3. The initial rates of butadiene formation were found to increase in the following order Ag/Zr(1.3)BEA(19) < Ag/Zr(2.1)BEA(25) < Ag/Zr(3.3)BEA(38) ≈ Ag/Zr(3.5)BEA(75). The comparison of the results with Ag/Zr(1.5)BEA-HT indicates a 2- to 3-fold higher activity of the materials obtained by post-synthesis treatment (Table 3).

Our previous studies on the synthesis of butadiene from ethanol[24,25] indicated that Zr open Lewis sites played a key

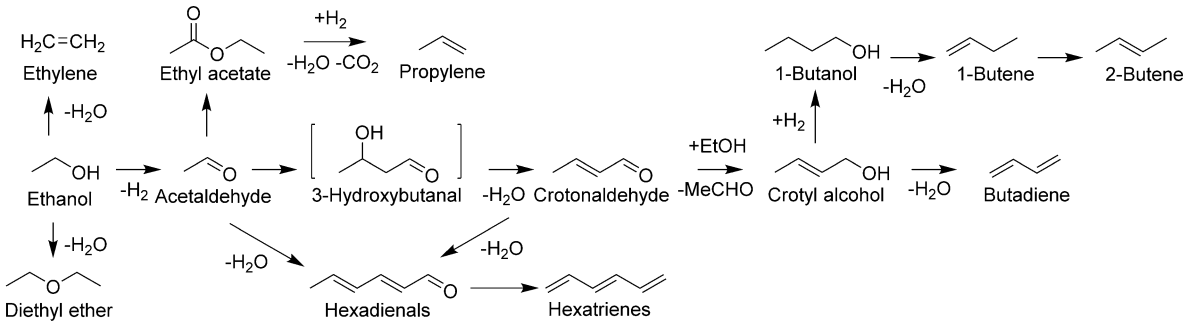

Scheme 3. Main reaction pathways.

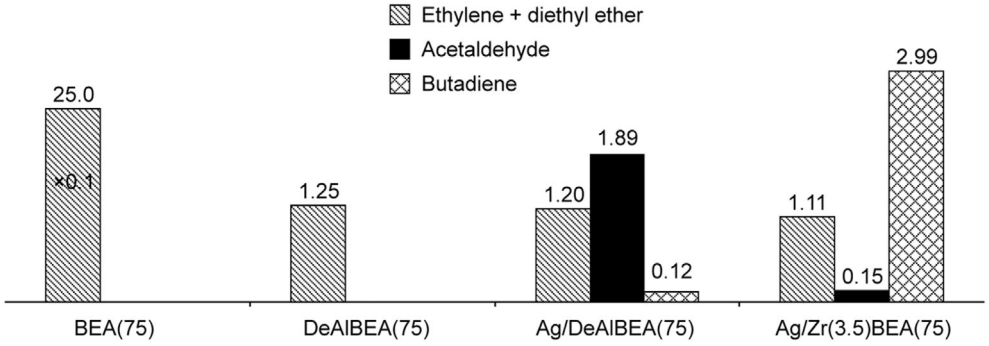

Figure 7. Initial formation rates of butadiene, acetaldehyde and dehydration products over BEA(75), DeAlBEA(75), Ag/DeAlBEA(75) and Ag/Zr(3.5)BEA(75) catalysts.

Table 3. Initial butadiene formation rates, ethanol conversions and products distribution over Ag-doped ZrBEA catalysts ($T = 593$ K, time on stream = 3 h).

Sample	Initial formation rate [μmol g^{-1} s^{-1}]	Ethanol conversion [%]	Selectivities [mol %]							
			butadiene	ethylene	propylene	butenes	ethyl ether	ethyl acetate	1-butanol	C_6+
Ag/Zr(1.3)BEA(19)	1.81	14.3	62.2	8.1	2.0	5.0	10.2	2.4	0.8	9.3
Ag/Zr(2.1)BEA(25)	2.25	15.9	61.1	8.3	2.0	4.9	10.0	2.5	0.4	10.8
Ag/Zr(3.3)BEA(38)	2.90	15.0	60.3	8.9	1.8	5.2	10.5	2.0	0.7	10.6
Ag/Zr(3.5)BEA(75)	2.99	14.9	58.7	9.8	1.9	5.0	11.9	2.2	0.6	9.9
Ag/Zr(1.5)BEA-HT	1.32	15.5	67.1	1.9	2.3	6.6	5.9	4.0	1.4	10.8

role in this process. Our current study confirms the above conclusion: the order of catalyst activity correlates linearly with the relative amount of open Lewis acid sites determined by FTIR (Figure 8). The order of the activity also correlates with the total Zr content in the samples (Figure S7), which can be expected because of the correlation between the amount of Zr open sites and Zr content (Table 2). The only sample that does not correlate is the Zr(1.5)BEA-HT catalyst, which has a significant amount of closed sites that have been shown to be less active for this reaction.[25] This sample has the lowest butadiene formation rate per Zr atom, hence confirming the higher activity of the open sites (Figure S7). All these observations support our previous conclusion on the high importance of open Lewis sites for the activity of the catalyst.[25]

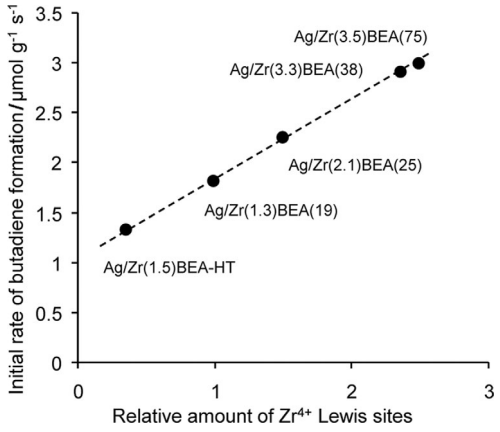

Figure 8. Initial butadiene formation rate versus relative amount of open Lewis sites measures by FTIR of adsorbed CO.

The analysis of the product distribution and selectivity of the catalysts was performed at similar conversion levels of ethanol (Table 3). Similar ethanol conversions of 14–16% were achieved by variation of the WHSV in the range of 1.2–3 g g^{-1} h^{-1}. The results show that ZrBEA catalysts obtained by post-synthesis had a selectivity towards butadiene in the range of 59–62%, which is close to the selectivity of ZrBEA-HT (67%). This observation suggests that the Zr^{4+} sites located in the molecular sieve frameworks exhibit the same selectivity in the overall reaction regardless of the method of incorporation: post-synthetic treatment or hydrothermal synthesis. However, some differences are observed for ethanol dehydration products such as diethyl ether and ethylene, the content of which was higher when using Ag/Zr(*y*)BEA(*x*) catalysts obtained by post-synthesis methods (Table 3). This result is most probably owing to traces of Brønsted acid sites in these samples, as evidenced by the FTIR spectra of adsorbed CO (Figure 6, Table 2). A small amount of Brønsted acid sites promotes the ethanol dehydration reactions, which leads to higher selectivity towards ethylene and diethyl ether. The increase of ethanol conversion increases the amount of these products, which is in line with our previous study.[49]

The comparison of different Ag-doped ZrBEA samples obtained by post-synthesis shows that the highest butadiene formation rate of 3 μmol g^{-1} s^{-1} is achieved over Ag/Zr(3.5)BEA(75). This value is two times higher than that obtained over Ag/ZrBEA-HT. The productivity of Ag/Zr(3.5)BEA(75) under the steady state conditions is estimated to be 0.58 g g^{-1} h^{-1}. To the best of our knowledge, this is the highest value obtained so far for a one step butadiene process and

approaches those achieved in a two-step process (350 mg L^{-1} h^{-1}).[29]

Conclusions

A new approach for the preparation of highly efficient Ag/ZrBEA catalyst for butadiene synthesis from ethanol has been proposed. The method involves post-synthetic treatment of dealuminated BEA zeolite with $ZrOCl_2$ in DMSO solution under reflux conditions. The FTIR and ^{29}Si MAS NMR analysis indicates that the terminal isolated silanol groups are involved in the Zr grafting process. Silanol nests generated during the dealumination of BEA have a very low, if any, contribution to Zr grafting. The materials obtained contain only open Zr Lewis sites ($Zr(OSi)_3OH$) as confirmed by FTIR spectroscopy of adsorbed carbon monoxide. Closed Zr Lewis sites are not detected, probably owing to the low involvement of silanol nests in the grafting process.

The content of the open Lewis sites correlates with the amount of Zr atoms grafted. It does not depend on the concentration of Al in the parent zeolite or the amount of nests formed during the dealumination. On the contrary, it is governed by the size of the zeolite crystal; the smaller the crystal size, the higher the amount of terminal silanols, the higher the content of Zr Lewis sites.

It is proposed that the post-synthetic treatment of dealuminated BEA zeolite with $ZrOCl_2$ in DMSO leads to Zr grafting preferentially to the terminal silanols on the external surface of the zeolite crystals, which yields highly accessible $Zr(OSi)_3OH$ open sites with high Lewis acidity. These sites are shown to be extremely active in the synthesis of butadiene from ethanol. The initial rates of ethanol conversion into butadiene over Ag-promoted ZrBEA catalysts shows a linear correlation with the amount of these sites. The Ag/ZrBEA catalysts synthesized using the post-synthesis modification show significant advantages over Ag/ZrBEA catalysts synthesized by a conventional hydrothermal procedure.

The best catalyst performance in terms of butadiene formation rate (3 μmol g^{-1} s^{-1}) was observed over Ag(3.5)/ZrBEA(75), which has the smallest crystal size and the highest content of Zr open sites. This catalyst shows the highest productivity of butadiene synthesis (0.58 g g^{-1} h^{-1}) under steady state conditions at a selectivity close to 60%.

Experimental Section

Preparation of the catalysts

BEA zeolites with a Si/Al ratio of 19, 25, 38 and 75 (supplied by Zeolyst and denoted as BEA(*x*), where *x* is the Si/Al ratio) were dealuminated by stirring 10 g of the parent material in 300 mL of 10 M aqueous HNO_3 solution at 363 K for 8 h. The resultant suspensions were diluted with 1 L H_2O and filtered. The samples were washed thoroughly with water and dried at 333 K overnight. The dealumination procedure was repeated four times. The samples were designated as DeAlBEA(*x*), where *x* is Si/Al ratio in the parent zeolite.

Before the introduction of zirconium, the dealuminated zeolites were activated for 8 h at 423 K to remove adsorbed water. The samples (3 g) were then added to a solution of 24.0 g of $ZrOCl_2 \cdot 8H_2O$ in 170 g of DMSO. The solution was heated at 403 K for 12 h and then added to 1 L of deionized water. The final suspension was filtered, rinsed with water and dried at 353 K. The calcination procedure was as follows: ramp at 3 K min^{-1} to 473 K, dwell for 6 h, ramp at 3 K min^{-1} to 823 K and dwell for 6 h. The samples were designated as Zr(*y*)BEA(*x*), were *x* is Si/Al ratio in the parent zeolite and *y* corresponds to the Zr content (in wt%) in the sample.

The hydrothermal synthesis of ZrBEA zeolite with a Si/Zr ratio of 100 was performed according to a previously reported procedure.[50] The as-synthesized material was calcined at 823 K for 5 h under a flow of dry air. The sample was denoted as ZrBEA-HT.

All catalysts were doped with 1 wt% of silver by incipient wetness impregnation with a $AgNO_3$ solution followed by calcination and reduction under a flow of hydrogen. Elemental analysis confirmed the silver content to be within 0.9–1.1 wt%. After the introduction of silver, "Ag/" was added as a prefix to the name of the catalyst.

Catalyst characterization

The elemental analysis was performed using energy dispersive X-ray fluorescence spectroscopy (EDXRF). Prior to the analysis the samples were mixed with $B(OH)_3$ and pressed in self-supporting wafers. The wafers were analyzed using a Thermo Scientific ARL Perform'x WDXRF spectrometer. N_2 sorption–desorption isotherms were measured at 77 K using a Micromeritics ASAP-2000 automatic surface area and pore size analyzer. Scanning electron microscopy (SEM) images of samples were obtained on a LEO EVO 50XVP (Zeiss) microscope. Powder X-ray diffraction (XRD) patterns of the samples were recorded on a Bruker PHASER D2 diffractometer using CuK_α radiation at a wavelength of 1.5456 Å. ^{29}Si solid-state MAS (magnetic angle spinning) NMR spectroscopy was performed using a Bruker Avance-400 spectrometer, operating at a resonance frequency of 79.46 MHz with a spinning rate of 10 kHz, pulse length of 3 μs, and recycle time of 20 s. The ^{29}Si chemical shifts are reported relative to tetramethylsilane.

The acidic properties were studied by FTIR spectroscopy of the adsorbed CO. IR spectra were recorded on a Nicolet Protégé 460 FTIR spectrometer at a 4 cm^{-1} optical resolution. Prior to the measurements, the catalysts were pressed in self-supporting discs and activated in the IR cell attached to a vacuum line at 723 K for 4 h. A low temperature vacuum cell cooled with liquid nitrogen was used for CO adsorption measurements. The pressure was measured by a Barocell gauge. Difference spectra were obtained by the subtraction of the spectra of the activated samples from the spectra of samples with the adsorbate. The subtraction was performed using the OMNIC 7.3 software package.

Evaluation of catalyst performance

Catalytic experiments were performed in a flow-type fixed-bed reactor under atmospheric pressure. In a typical experiment, 2 g of catalyst (size fraction 0.5–1 mm) was packed into the quartz tubular reactor and purged with nitrogen at 873 K for 0.5 h followed by subsequent reduction in a flow of hydrogen at 593 K. Ethanol (95 wt%) was used as a feed. The reaction mixture was fed using a syringe pump (Razel). Helium was used as a carrier gas (molar ratio EtOH/He = 1). The weight hourly space velocity (WHSV) was varied from 1.2 to 3.0 h^{-1}, the reaction temperature was 593 K. Gaseous products were analyzed on a Crystal 2000M gas chroma-

tograph using a 50 m SE-30 column. Liquid products were separated and analyzed using 50 m SE-30 and 2 m Porapak Q columns. Methane was used as an external standard for gaseous products. The conversion of ethanol, selectivity and yields of the products were calculated as follows:

$$\text{Ethanol conversion} = \frac{m_{\text{reacted(EtOH)}}}{m_{\text{fed(EtOH)}}} \times 100\% \quad (1)$$

$$\text{Selectivity} = \frac{k_j^F \frac{m_j}{Mr_j} \times 100\%}{m_{\text{reacted(EtOH)}}/46} \quad (2)$$

$$\text{Yield} = \text{Ethanol conversion} \times \text{Selectivity}/100, \quad (3)$$

where m_j is the mass of product j in the reaction mixture, Mr_j is the molecular weight of product j, and k_j^F is the number of ethanol molecules required for the production of product j.

The initial rate of butadiene formation was calculated from the initial slope of the kinetic curves in the range of ethanol conversion from 4–15%. The variation of ethanol conversion was achieved by changing the WHSV from 1.2–15 h^{-1}. The data were collected under steady state conditions after 3 h on stream.

Acknowledgements

The authors thank the Russian Science Foundation for the financial support (Grant No 14-23-00094) and Mr. Andrey Ivanov for NMR measurements.

Keywords: butadiene · domino reaction · heterogeneous catalysis · zeolites · zirconium

[1] Y. Román-Leshkov, M. E. Davis, *ACS Catal.* **2011**, *1*, 1566 – 1580.
[2] M. Moliner, *Dalton Trans.* **2014**, *43*, 4197 – 4208.
[3] A. Corma, L. T. Nemeth, M. Renz, S. Valencia, *Nature* **2001**, *412*, 423 – 425.
[4] M. S. Holm, S. Saravanamurugan, E. Taarning, *Science* **2010**, *328*, 602.
[5] J. J. Pacheco, M. E. Davis, *Proc. Natl. Acad. Sci. USA* **2014**, *111*, 8363.
[6] T. De Baerdemaeker, B. Steenackers, D. De Vos, *Chem. Commun.* **2013**, *49*, 7474.
[7] S. Van de Vyver, Y. Román-Leshkov, *Angew. Chem. Int. Ed.* **2015**, *54*, 12554 – 12561; *Angew. Chem.* **2015**, *127*, 12736 – 12744.
[8] A. Corma, M. E. Domine, S. Valencia, *J. Catal.* **2003**, *215*, 294 – 304.
[9] H. Y. Luo, D. F. Consoli, W. R. Gunther, Y. Román-Leshkov, *J. Catal.* **2014**, *320*, 198 – 207.
[10] M. Boronat, A. Corma, M. Renz, *J. Phys. Chem. B* **2006**, *110*, 21168 – 21174.
[11] V. Sushkevich, I. Ivanova, S. Tolborg, E. Taarning, *J. Catal.* **2014**, *316*, 121 – 129.
[12] S. Van de Vyver, C. Odermatt, K. Romero, T. Prasomsri, Y. Román-Leshkov, *ACS Catal.* **2015**, *5*, 972 – 977.
[13] D. Lewis, S. Van de Vyver, Y. Román-Leshkov, *Angew. Chem. Int. Ed.* **2015**, *54*, 9835 – 9838; *Angew. Chem.* **2015**, *127*, 9973 – 9976.
[14] M. Moliner, Y. Román-Leshkov, M. E. Davis, *Proc. Natl. Acad. Sci. USA* **2010**, *107*, 6164 – 6168.
[15] Y. Román-Leshkov, M. Moliner, J. A. Labinger, M. E. Davis, *Angew. Chem. Int. Ed.* **2010**, *49*, 8954 – 8957; *Angew. Chem.* **2010**, *122*, 9138 – 9141.
[16] M. S. Holm, Y. J. Pagan-Torres, S. Saravanamurugan, A. Riisager, J. A. Dumesic, E. Taarning, *Green Chem.* **2012**, *14*, 702 – 706.
[17] R. Bermejo-Deval, R. Gounder, M. E. Davis, *ACS Catal.* **2012**, *2*, 2705 – 2713.
[18] R. Gounder, M. E. Davis, *J. Catal.* **2013**, *308*, 176 – 188.
[19] J. Dijkmans, D. Gabriels, M. Dusselier, F. de Clippel, P. Vanelderen, K. Houthoofd, A. Maliet, Y. Pontikes, B. F. Sels, *Green Chem.* **2013**, *15*, 2777 – 2785.
[20] W. R. Gunther, Y. Wang, Y. Ji, V. K. Michaelis, S. T. Hunt, R. G. Griffin, Y. Román-Leshkov, *Nat. Commun.* **2012**, *3*, 1109.
[21] E. Taarning, S. Saravanamurugan, M. S. Holm, J. Xiong, R. M. West, C. H. Christensen, *ChemSusChem* **2009**, *2*, 625 – 627.
[22] C. Hammond, S. Conrad, I. Hermans, *Angew. Chem. Int. Ed.* **2012**, *51*, 11736 – 11739; *Angew. Chem.* **2012**, *124*, 11906 – 11909.
[23] M. Dusselier, P. Van Wouwe, A. Dewaele, E. Makshina, B. F. Sels, *Energy Environ. Sci.* **2013**, *6*, 1415 – 1442.
[24] V. Sushkevich, I. Ivanova, E. Taarning, *Green Chem.* **2015**, *17*, 2552 – 2559.
[25] V. Sushkevich, D. Palagin, I. Ivanova, *ACS Catal.* **2015**, *5*, 4833 – 4836.
[26] A. D. Patel, K. Meesters, H. den Uil, E. de Jong, K. Bloka, M. K. Patel, *Energy Environ. Sci.* **2012**, *5*, 8430 – 8444.
[27] J. A. Posada, A. D. Patel, A. Roes, K. Blok, A. C. Faaij, M. K. Patel, *Bioresour. Technol.* **2013**, *135*, 490 – 499.
[28] C. Angelici, B. M. Weckhuysen, P. Bruijnincx, *ChemSusChem* **2013**, *6*, 1595 – 1614.
[29] E. V. Makshina, M. Dusselier, W. Janssens, J. Degrève, P. Jacobs, B. Sels, *Chem. Soc. Rev.* **2014**, *43*, 7917 – 7953.
[30] J. Wang, K. Okumura, S. Jaenicke, G.-K. Chuah, *Appl. Catal. A* **2015**, *493*, 112 – 120.
[31] C. Chang, C. Chu, J. Miale, R. F. Bridger, R. B. Calvert, *J. Am. Chem. Soc.* **1984**, *106*, 8143 – 8146.
[32] K. Yamagishi, S. Namba, T. Yashima, *J. Phys. Chem.* **1991**, *95*, 872 – 877.
[33] W. Ren, Z. Hu, T. Ge, X. Zhou, L. Chen, Y. Zhu, J. Shi, *Chin. J. Catal.* **2015**, *36*, 906 – 912.
[34] B. Tang, W. Dai, X. Sun, N. Guan, L. Li, M. Hunger, *Green Chem.* **2014**, *16*, 2281 – 2291.
[35] P. Wu, T. Komatsu, T. Yashima, S. Nakata, H. Shouji, *Microporous Mater.* **1997**, *12*, 25 – 37.
[36] P. Li, G. Liu, H. Wu, Y. Liu, J.-g. Jiang, P. Wu, *J. Phys. Chem. C* **2011**, *115*, 3663 – 3670.
[37] W. N. P. van der Graaff, G. Li, B. Mezari, E. A. Pidko, E. J. M. Hensen, *ChemCatChem* **2015**, *7*, 1152 – 1160.
[38] B. Tang, W. Dai, G. Wu, N. Guan, L. Li, M. Hunger, *ACS Catal.* **2014**, *4*, 2801 – 2810.
[39] J. Dijkmans, M. Dusselier, W. Janssens, M. Trekels, A. Vantomme, E. Breynaert, C. E. A. Kirschhock, B. F. Sels, *ACS Catal.* **2016**, *6*, 31 – 46.
[40] J. Dijkmans, J. Demol, K. Houthoofd, S. Huang, Y. Pontikes, B. Sels, *J. Catal.* **2015**, *330*, 545 – 557.
[41] J. Dijkmans, D. Gabriëls, M. Dusselier, K. Houthoofd, P. C. M. M. Magusin, S. Huang, Y. Pontikes, M. Trekels, A. Vantomme, L. Giebeler, S. Oswald, B. F. Sels, *ACS Catal.* **2015**, *5*, 928 – 940.
[42] B. Tang, W. Dai, X. Sun, G. Wu, N. Guan, M. Hunger, L. Li, *Green Chem.* **2015**, *17*, 1744 – 1755.
[43] P. Wolf, C. Hammond, S. Conrad, I. Hermans, *Dalton Trans.* **2014**, *43*, 4514 – 4519.
[44] E. B. Lami, F. Fajula, D. Anglerot, T. Des Courieres, *Microporous Mater.* **1993**, *1*, 237 – 245.
[45] V. Ordomsky, V. Murzin, Yu. Monakhova, Y. Zubavichus, E. Knyazeva, N. Nesterenko, I. Ivanova, *Microporous Mesoporous Mater.* **2007**, *105*, 101 – 110.
[46] K. Hadjiivanov, *Adv. Catal.* **2014**, *57*, 99 – 318.
[47] V. Sushkevich, A. Vimont, A. Travert, I. Ivanova, *J. Phys. Chem. C* **2015**, *119*, 17633 – 17639.
[48] K. Hadjiivanov, G. Vayssilov, *Adv. Catal.* **2002**, *47*, 307 – 511.
[49] V. Sushkevich, I. Ivanova, V. Ordomsky, E. Taarning, *ChemSusChem* **2014**, *7*, 2527 – 2536.
[50] S. H. Liu, S. Jaenicke, G. K. Chuah, *J. Catal.* **2002**, *206*, 321 – 330.

Received: April 29, 2016
Published online on ■■ ■■, 0000

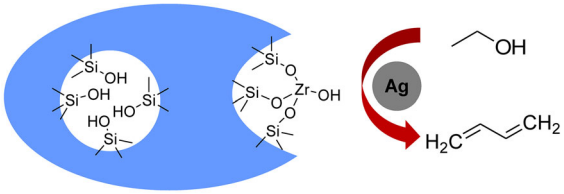

*V. L. Sushkevich, I. I. Ivanova**

■■ – ■■

Ag-Promoted ZrBEA Zeolites Obtained by Post-Synthetic Modification for Conversion of Ethanol to Butadiene

The Ag goes to Zeolites! Ag/ZrBEA (zirconium-containing zeolite beta) catalysts prepared using a post-synthesis method show significant advantages compared with Ag/ZrBEA catalysts synthesized using a conventional hydrothermal procedure. Parent AlBEA materials with different Si/Al ratios and crystal sizes are used to determine the best catalyst for the conversion of ethanol to butadiene.